Deciphering the multi-step degradation mechanisms of carbonate-based electrolyte in Li batteries

Gregory Gachot [a], Sylvie Grugeon [a], Michel Armand [a], Serge Pilard [b],
Pierre Guenot [c,1], Jean-Marie Tarascon [a], Stephane Laruelle [a,*]

[a] *LRCS, Université de Picardie Jules Verne, 33 rue de Saint Leu, 80039 Amiens, France*
[b] *Plate-Forme Analytique, Université de Picardie Jules Verne, Amiens, France*
[c] *Centre Régional de Mesures Physiques de l'Ouest, Université de Rennes 1, Rennes, France*

We would like to dedicate this article to Pierre Guenot, our Mass Spectrometry mentor, who tragically passed away during the course of this study.

Abstract

Electrolytes are crucial to the safety and long life of Li-ion batteries, however, the understanding of their degradation mechanisms is still sketchy. Here we report on the nature and formation of organic/inorganic degradation products generated at low potential in a lithium-based cell using cyclic and linear carbonate-based electrolyte mixtures. The global formation mechanism of ethylene oxide oligomers produced from EC/DMC (1/1 w/w)–LiPF$_6$ salt (1 M) electrolyte decomposition is proposed then mimicked via chemical tests. Each intermediary product structure/formula/composition is identified by means of combined NMR, FTIR and high resolution mass spectrometry (ESI-HRMS) analysis. The key role played by lithium methoxide as initiator of the electrolyte degradation is evidenced, but more importantly we isolated for the first time lithium methyl carbonate as a side product of the ethylene oxide oligomers chemical formation. The same degradation mechanism was found to hold on for another cyclic and linear carbonate-based electrolyte such as EC/DEC (1/1 w/w)–LiPF$_6$ salt (1 M). Such findings have important implications in the choice of chemical additives for developing highly performing electrolytes.
© 2007 Elsevier B.V. All rights reserved.

Keywords: Mass spectrometry; Li-ion batteries; Carbonate-based electrolyte; Electrolyte degradation; Ring-opening nucleophilic reactions

1. Introduction

The Li-ion battery technology, which is considered as the "lead–acid technology" of the 21st century, has conquered the portable electronics market, and is on the verge of entering the automotive industry. For the latter application it is imperative to enhance its energy and power density and lower its cost without comprising safety or calendar life. Undoubtedly, the future of Li-ion technology will rely on a sound understanding of electrolyte components as we move to the next generation of either positive electrodes based on higher voltages (5 V) insertion materials or negative non-insertion electrodes (e.g., Li-alloying or conversion reactions) making use of nanomaterials. Novel strategies to

harmoniously couple the next generation of cathodes or anodes with today's electrolytes will have to be found. Conducting such a research requires to secure/adjust past beliefs regarding the basic understanding of electrode/electrolyte interfaces, and also to set new experimental protocols to better analyze the electrolyte degradation products in either a passive (*in situ*) or active way (post-mortem).

Owing to their combined properties of ion solvation, electrochemical stability and their ability to form stable and protective layers, alkyl carbonate-based electrolyte solutions are used in most of today's commercial Li-ion cells. These electrolytes are usually composed of both linear carbonate-like dimethyl carbonate (DMC), diethyl carbonate (DEC) or ethyl methyl carbonate (EMC), and cyclic carbonate-like ethylene carbonate (EC) or propylene carbonate (PC) to combine different properties like viscosity and conductivity. These carbonates can trigger electrochemical and chemical reactions to form a passivating layer commonly named SEI [1] favourable to the well functioning of
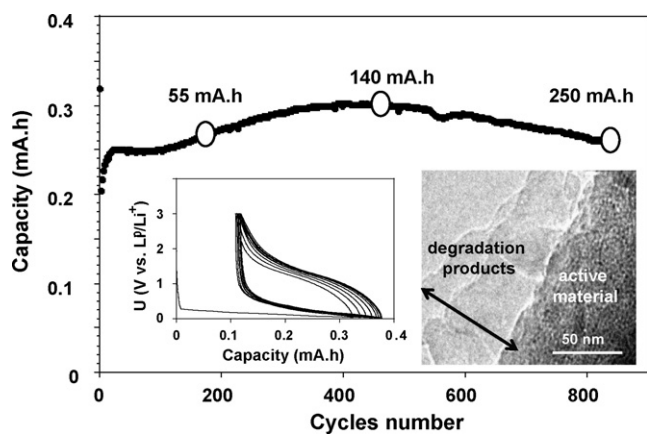

Fig. 1. Capacity retention of a treated stainless steel/Li cells plotted as a function of the cycles number. The three circles correspond to the total accumulated discharge capacity of cells whose separator electrolyte degradation products have been analyzed by ESI-HRMS. Inset 1: SEM micrograph of a Cr-based conversion active material/electrolyte interface showing degradation product layer surrounding nanomaterials composite at the discharged state (metallic nanoparticles embedded in Li_2O matrix). Inset 2: Charge/discharge voltage–capacity trace for a SUS316L stainless steel disc treated at $700\,^{\circ}C$ under H_2/N_2 for 16 h/Li^0 cell.

the carbon-based negative electrodes in today's Li-ion batteries. Although limited, such electrolytes are not free of side-reactions, whose basic understanding is still very sketchy despite a large number of studies. Research on this topic is complex and is rendered somewhat difficult as the SEI formation usually involves very small amount of material.

With the advent of nanomaterial-based negative electrodes based on either Li-alloying or conversion reactions, which are

tion processes and shedding new light on the reacting paths by which they occur. To carry out such a study, thorough analytical post-mortem studies of degradation products, recovered at the working electrode/electrolyte interfaces or within the separator of cycled "lithium/conversion electrodes" half-cells were used. Chromium-based oxide (named CBO) grown on stainless steel mesh tissues [4] was chosen as our conversion electrode material due to its large sustainable reversible capacity (Fig. 1), but more importantly for its low functioning voltage vs. Li^0/Li^+ (inset 1; Fig. 1) in order to generate copious amounts of electrolyte degradation products upon cycling as shown (inset 2; Fig. 1). For the electrolyte we mainly selected an EC/DMC (1/1 w/w)–$LiPF_6$ salt (1M) mixture because it is one of the most commonly used worldwide in laboratory test cells; and surprisingly it is one for which degradation reactions mechanisms were, to our knowledge, never clearly sorted out, although pieces and parts of the reacting degradation puzzle have been reported in the literature [5–18]. For instance, it is well known that, according to the published reaction schemes listed below, electrochemical reduction mechanisms of EC and DMC lead to inorganic lithium salts formation such as lithium carbonate, lithium methoxide and lithium methyl carbonate.
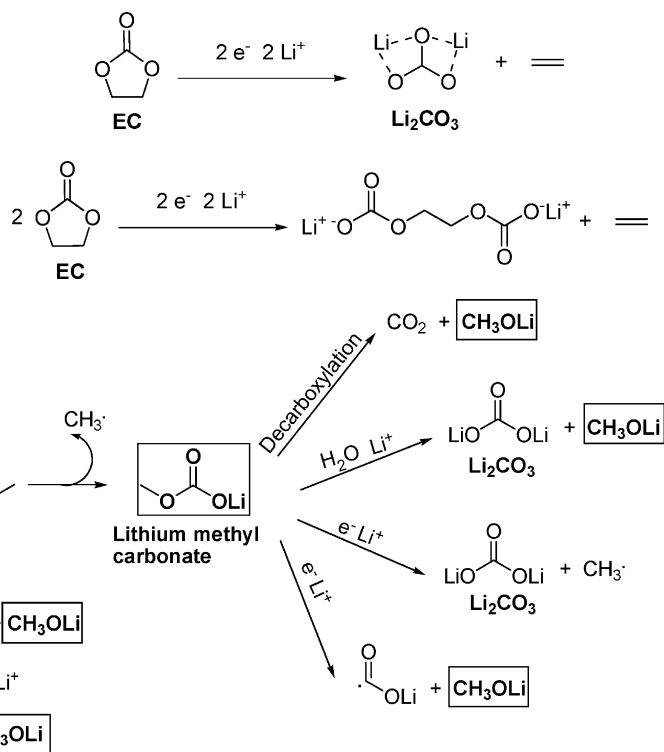
usually characterized by impressive capacity gains over classical carbonaceous electrodes, such a situation has drastically changed as these nanocomposite electrodes were shown to strongly enhance classical electrolyte degradation resulting in the formation of large amounts of inorganic and organic compounds [2,3]. While such degradation products can turn out to be detrimental to both the battery safety and calendar life, they offer unprecedented opportunities to revisit the electrolyte decomposition mechanisms. We decided to seize this opportunity in the dual hope of lowering nanomaterial-driven electrolyte degrada-

Nevertheless this aforementioned view does not take into account the overall reported spectrum of decompositions products with namely the presence of oxy-ethylene unit-based polymers spotted by other groups through gas chromatography/low resolution mass spectrometry [17] or XPS [19,20] with the first truly identified member being the dimethyl 2,5-dioxahexane dicarboxylate (DMDOHC) compound. Therefore, the chemical formation mechanism of such an entity remains quite controversial and subject to debate. For instance, Yamachi and co-workers suggested a trans-esterification mechanism from

EC and DMC [15] (as shown below) while Ogumi and co-workers proposed an EC attack by a methoxide anion [17].

$$EC + DMC \longleftrightarrow$$

DMDOHC

As far as the polymers are concerned, Sloop et al. [21] proposed, according to the reaction below, an acid-catalyzed EC ring-opening reaction to account for their formation.

EC

$$\xrightarrow{85\,^{\circ}C}$$

More recently, by performing post-mortem analyses on a separator recovered from a long-term cycled (200 cycles) Li/CBO, our group provided direct experimental evidence, by means of infrared and high resolution mass spectrometry (ESI-HRMS) techniques, for the simultaneous presence of lithium methyl carbonate and of some ethylene oxide oligomers ($n < 10$) having various end groups (hydroxy, methoxy, carbonate and phosphate) as part of the electrolyte degradation products. To make further progress, as reported in this publication, we propose an experimentally supported chemical/electrochemical reaction pathway mechanism capable of reconciling all the established experimental facts, namely the formation of the oligomers in conjunction with lithium inorganic salts. A specific feature of the present paper is that each proposed mechanism process is mimicked by chemical tests with the end products identified either by high resolution mass spectrometry, IR or NMR analyses. Among others, the paper highlights (i) how the formation of these oligomers could be responsible for the subsequent precipitation of inorganic salts such as lithium methyl carbonate and (ii) how the proposed degradation mechanism could be generalized to mixture of cyclic and linear carbonate-based electrolytes by studying EC/DEC (1/1 w/w)–LiPF$_6$ salt (1 M)-based cycled cells.

2. Experimental

2.1. Cells assembly

Coin cells (standard 2035-size) were assembled in an argon-filled dry glove box (Fig. 2). The working electrode consists of one 2 cm^2 SUS316L-type stainless steel disc treated at 700 °C under H$_2$/N$_2$ atmosphere during 16 h to favour the growth of a 300–500 nm chromium oxide layer at its surface. It is separated from a lithium foil piece used as the negative electrode by a borosilicate micro-fiber (Millipore) film impregnated with 0.5 ml of electrolyte solution (battery grade quality). Once assembled, coin cells were placed into an oven at 55 °C and cycled between 0.02 and 3 V in galvanostatic mode (0.15 mA cm^{-2}) using a Mac Pile (Biologic, Claix, France) system. The cells were stopped at the end of a charge state (3 V) once

Fig. 2. Cross-sectional view of a "treated stainless steel/lithium foil" coin cell.

an accumulated discharge capacity of 55, 140 or 250 mAh was reached (Fig. 1). The cell was then put back into the glove box to be carefully opened. The separator was recovered, washed with acetonitrile (<10 ppm water) and the supernatant was analyzed by high resolution mass spectrometry. Chemical experiments have been performed in glass test tubes under argon at 55 °C. After being subjected to different storage times, the solution was diluted in acetonitrile and analyzed by ESI-HRMS, and insoluble products were analyzed by IR and NMR spectroscopy.

LP30 battery grade, EC and DEC "selectipur" were purchased from Merk. Lithium hexafluorophosphate battery grade and lithium methoxide were purchased from Sigma–Aldrich.

2.2. ESI-HRMS measurements

ESI-HRMS experiments were performed in the positive ion mode on a Q-TOF Ultima Global instrument (Waters-Micromass, Manchester, UK) equipped with a pneumatically assisted electrospray ion source (Z-spray) and an additional sprayer for the reference compound (LockSpray). The prepared solutions were directly introduced (5 μL min^{-1}) via an integrated syringe pump in the electrospray source. The source and desolvation temperatures were kept at 80 and 150 °C, respectively. Nitrogen was used as a drying and nebulizing gas at flow rates of 350 and 50 L h^{-1}, respectively. The capillary voltage was 2.5 kV, the cone voltage 100 V, and the rf lens 1 energy 60 V. Calibration of the instrument was performed using the ions produced by a phosphoric acid solution (0.2% in H$_2$O/CH$_3$CN 50/50 v/v). For accurate mass measurements a lock mass correction, using appropriate cluster ions of phosphoric acid [(H$_3$PO$_4$)$_n$ + H]$^+$, was applied. The mass range was 50–1000 Da and spectra were recorded at 1 s scan^{-1} in the profile mode at a resolution of 10,000 full width at half-maximum (FWMH). Data acquisition and processing were performed with MassLynx v 4.0 software.

2.3. FTIR/ATR measurement

Infrared spectra were recorded on a Nicolet Fourier transform infrared 510 spectrometer working in the 40,000–400 cm^{-1} spectra range, equipped with attenuated total reflectance technique (ATR) and a Ge crystal working in the 4000–700 cm^{-1} spectra range (resolution: 4 cm^{-1}).

Table 1
Degradation products with PEG chains recovered from the cell separator after cycling at 55 °C up to a total accumulated discharge capacity of 250 mAh

O–R₂	R₁		
	–CO₂Me	–Me	–H
–CO₂Me	Series 1_n	Series 2_n	Series 4_n
–Me	Series 2_n	Series 3_n	Series 5_n
–H	Series 4_n	Series 5_n	Series 6_n

2.4. NMR measurement

The NMR analyses were conducted on a BRUKER AVANCE 300 MHz spectrometer having quadruple probe and z-gradient spectrometer. Samples were prepared after compound dissolution in D_2O (99% Merck reagents industry). NMR spectra were recorded by tuning eight scans acquisition for the ^1H acquisition parameters. Spectra were recorded using D_2O as an internal standard. Data fittings were performed with X-Win-NMR-software.

3. Results and discussion

Let us first recall, in order to make what comes next in this paper more understandable, what has been clearly established in our earlier post-mortem identification of the inorganic and organic decomposition products recovered from a chromium oxide-based conversion material/lithium cell using EC/DMC (1/1 w/w)–LiPF₆ salt (1 M) electrolyte, cycled at 55 °C then stopped once an accumulated discharge capacity 250 mAh was reached [2,22]. Among the main finding was the presence at the working electrode material surface, as deduced by transmission electron microscopy, of a solid layer surrounded by a jelly-like film (inset Fig. 1) with (1) the solid layer consisting of numerous inorganic compounds such as lithium carbonate, lithium methyl carbonate, and lithium fluoride and (2) the jelly-like film mainly composed of ethylene oxide-based oligomers ($n < 10$). The latter, have identical PEOs units, differentiated solely by the nature of the termination groups leading to various 1_n, 2_n, 3_n, 4_n, 5_n and 6_n series (see Table 1) having carbonate/carbonate (series 1_n), carbonate/methoxy (series 2_n), methoxy/methoxy (series 3_n), carbonate/hydroxy (series 4_n), methoxy/hydroxy (series 5_n), and

hydroxyl/hydroxyl (series 6_n) R₂/R₁ ending groups (see below), respectively.
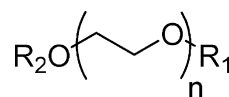
It is worth mentioning that the DMDOHC compound corresponding to the first member of the 1_n series reported in the literature [17], has not been detected under our extreme cycling conditions (800 cycles at 55 °C). At this juncture it is important to realize that this absent compound could simply be an intermediary species that does initially appear and then is consumed at a more advanced stage of the degradation process. To test this hypothesis, a similar cell was cycled at 55 °C and then stopped when an accumulated discharge capacity of only 55 mAh was reached. The separator was recovered, washed with acetonitrile and the supernatant was analyzed by high resolution mass spectrometry (Fig. 3). Not only was the dialkyl dicarbonate 1_1 $[M+Li]^+$ m/z 185,0637 identified but so were some oligomers of the 1_n and 4_n series suggesting that there is a link between the 1_1 compound and the other evidenced PEO series.

Ogumi and co-workers [17] suggested a reaction mechanism for the formation of the 1_1 compound (e.g., DMDOHC) by considering the three possible attacks of lithium alkoxide on a carbonate function (as shown below). Among them are two attacks on C_1 carbon with folding back of either the doublet on the oxygen of the methoxy function to reform MeOLi ("a" attack; solid arrow) or the doublet on the oxygen of the ether function to form new lithium alkoxide ("b" attack, dashed arrow), and a third one on the C_2 carbon with folding back of the doublet on the oxygen of the ether function to form lithium methyl carbonate ("c" attack).
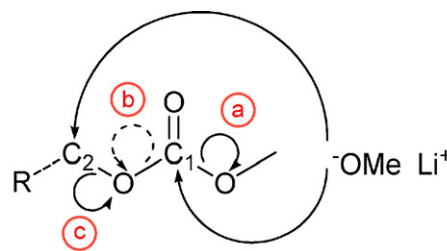
Possible attacks of lithium alkoxide on a carbonate function
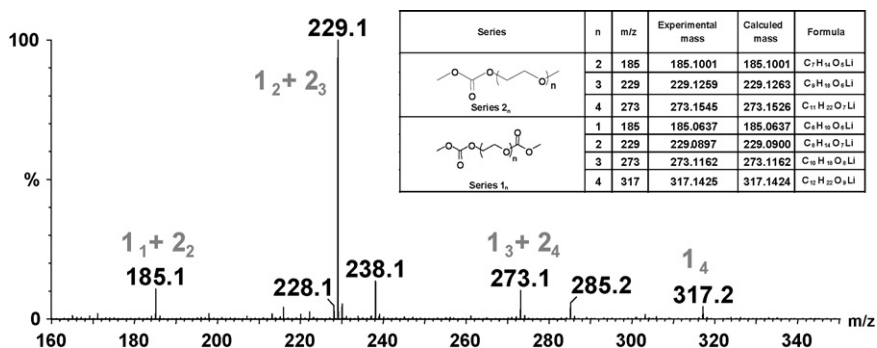
Fig. 3. ESI-HRMS spectrum of the degradation products recovered from the cell separator after cycling at 55 °C up to a total accumulated discharge capacity of 55 mAh.
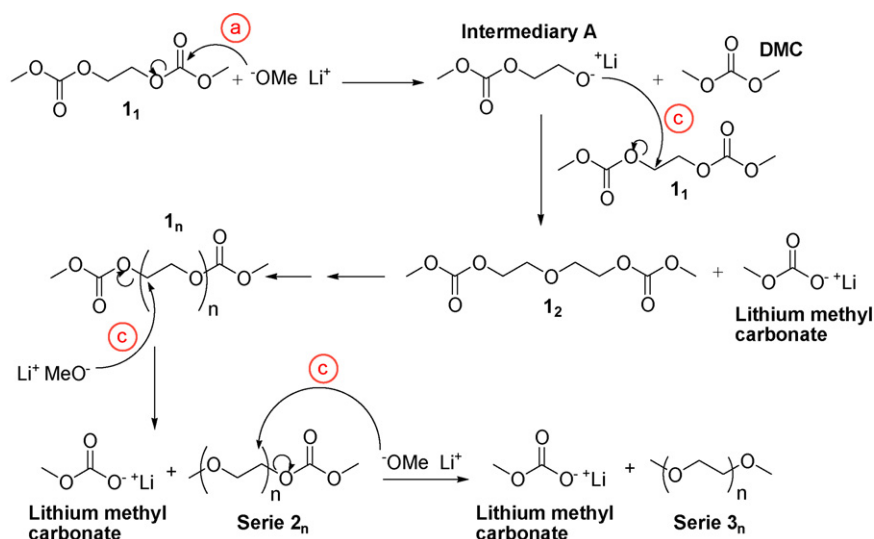
Fig. 4. Reaction scheme for series 1_n–3_n formation.

Based on these considerations, they suggested the "a" and "b" attacks, which are identical in the case of symmetric carbonate molecules such as EC, as being the most likely to explain the formation of the DMDOHC as shown below.
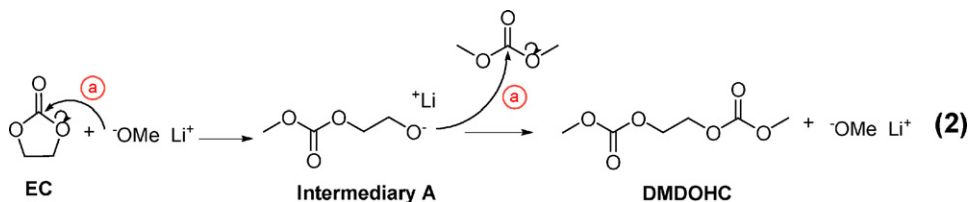
Generalizing these three different attack modes to non-symmetric carbonate molecules gives us the clue to suggest reaction mechanism paths (Fig. 4) for the formation of the 1_n, 2_n and 3_n series involving the reactivity of the 1_1 compound in the presence of MeOLi. First, an "a" attack of MeOLi leads to the formation of the intermediary A salt; it could then react via a "c" attack with 1_1 molecules to lengthen the PEO chain, and to give the 1_2 molecule with the possibility for this reaction to proceed to form the 1_n series. Afterwards, once the 1_n molecules have been formed, they can give birth, by MeOLi "c" attacks, to the 2_n and then 3_n series. Finally, it seems that all PEO oligomers result from chemical reactions initiated by electrochemical decomposition of the linear carbonate DMC into lithium methoxide. Therefore, the chemical reactivity of MeOLi, electrochemically formed upon reduction at low potential in Li-half-cells, has been up to now underestimated in literature.

On the basis of this conjuncture, and to experimentally support the aforementioned chronological mechanism established for the formation of the 1_n, 2_n, 3_n oligomers, we have undertaken a chemical simulation study of the MeOLi reactivity in the presence of electrolyte. An EC/DMC (1/1 w/w)–LiPF$_6$ (1 M) electrolyte mixture was stored at 55 °C in the presence of commercial MeOLi. For the sake of completion, two different MeOLi concentrations, one low (10^{-2} mol L^{-1}) and one high (1 M), were introduced into the electrolyte solution. Both solutions were kept for various lengths of time (1 day, 3 days, 2

weeks, and 1 month) at 55 °C under argon, and the degradation products formation kinetics were followed by high resolution mass spectrometry.

3.1. Storage tests for low MeOLi concentrations (10^{-2} mol L^{-1})

The ESI–MS spectra resulting from the stored samples are represented in Fig. 5. Note that the 1-month spectrum is not shown, as it is similar to that obtained after 2 weeks. The overall degradation products, accurate masses as well as their corresponding structural formula are reported in Table 2. As several compounds display very close masses, the high resolution was required to separate the isobaric ions and to their mass measurements. Fig. 6 clearly illustrates this experimental mass separation on the 7_1/1_3 compounds.

After 1 day, the 1_1 compound is identified, corroborating the notion that it is the first compound to form chemically. Upon increase of the reaction time, the peaks corresponding to the various members of the 1_n series show a progressive increase of the number of ethylene oxide units: 1_2 (m/z 229); 1_3 (m/z 273); 1_4 (m/z 317); 1_5 (m/z 361), came up. It is therefore worth mentioning that we could not monitor the 1_1 compound consumption throughout the experiment; this is due to an inherent limitation of the technique that always attributes the 100% intensity mass signal to the most intense peak. As the 1_1 compound peak turns out to always be the highest one, whatever the experiment duration time, it always appears as 100%.
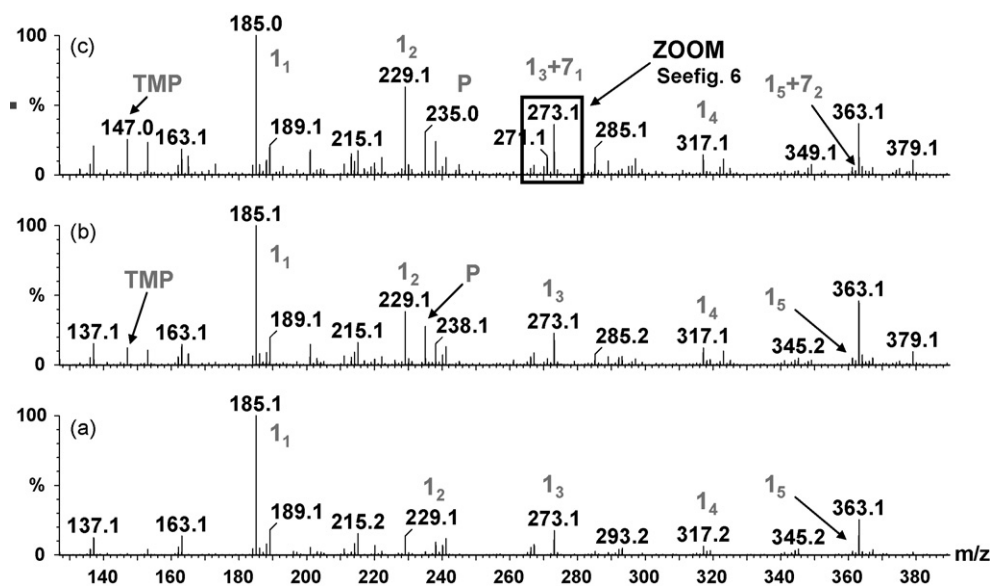
Fig. 5. ESI-HRMS spectra of EC/DMC (1/1 w/w)–LiPF$_6$ salt (1 M) solution with MeOLi (10^{-2} mol L^{-1}) stored at 55 °C for (a) 1 day, (b) 3 days and (c) 2 weeks.

In parallel to the 1_n series, the 3-day and 2-week storage spectrum evidenced the presence of trimethyl phosphate (TMP), PEO units with phosphate/carbonate ending groups (termed P) and ethylene carbonate chains (denoted series 7_n). This series was never observed before in electrolytes recovered from electrochemical cells, even after long cycling times at 55 °C. Such a difference could be nested in the electrolyte concentration difference between the electrochemical (1 M) and chemical (10^{-2} mol L^{-1}) tests. To account for the formation mechanism of this newly 7_n series, we went back to the early stage of our general mechanism scheme and simply considered that the intermediary A molecule could initially react with 1_1 via a nucleophilic "a" attack, and not a "c" attack as for the 1_n formation. Via this different path we can easily explain the formation of
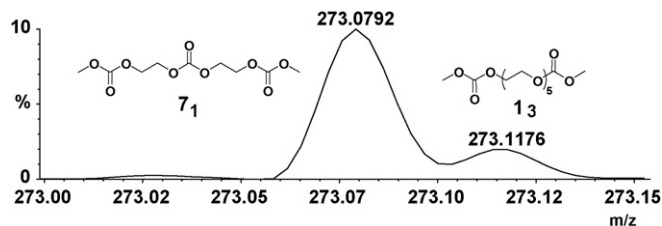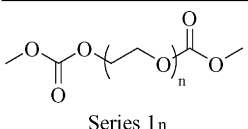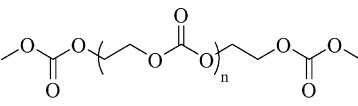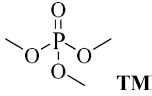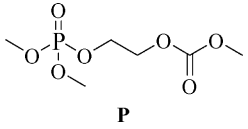
Fig. 6. Enlargement of high-resolution peaks m/z 273 (7_1 and 1_3).

the 7_1 compound. Thereafter, the lengthening of the ethylene carbonate chain involves two successive steps (Fig. 7); a "b" attack of the 7_1 product by MeOLi to form the intermediary B molecule, which subsequently reacts with 1_1 by an "a" attack.

Table 2
Degradation products formed in EC/DMC (1/1 w/w)–LiPF$_6$ salt (1 M) solution with MeOLi (10^{-2} mol L^{-1}) after 2-week storage at 55 °C

Series	n	m/z	Experimental mass	Calculated mass	Formula
Series 1$_n$	1	185	185.0637	185.0637	C$_6$H$_{10}$O$_6$Li
	2	229	229.0897	229.0900	C$_8$H$_{14}$O$_7$Li
	3	273	273.1176	273.1162	C$_{10}$H$_{18}$O$_8$Li
	4	317	317.1425	317.1424	C$_{12}$H$_{22}$O$_9$Li
	5	361	361.1685	361.1686	C$_{14}$H$_{26}$O$_{10}$Li
Series 7$_n$	1	273	273.0792	273.0798	C$_9$H$_{14}$O$_9$Li
	2	361	361.0963	361.0958	C$_{12}$H$_{18}$O$_{12}$Li
TMP		147	147.0397	147.0399	C$_3$H$_9$O$_4$PLi
P		235	235.0564	235.0559	C$_6$H$_{13}$O$_7$PLi
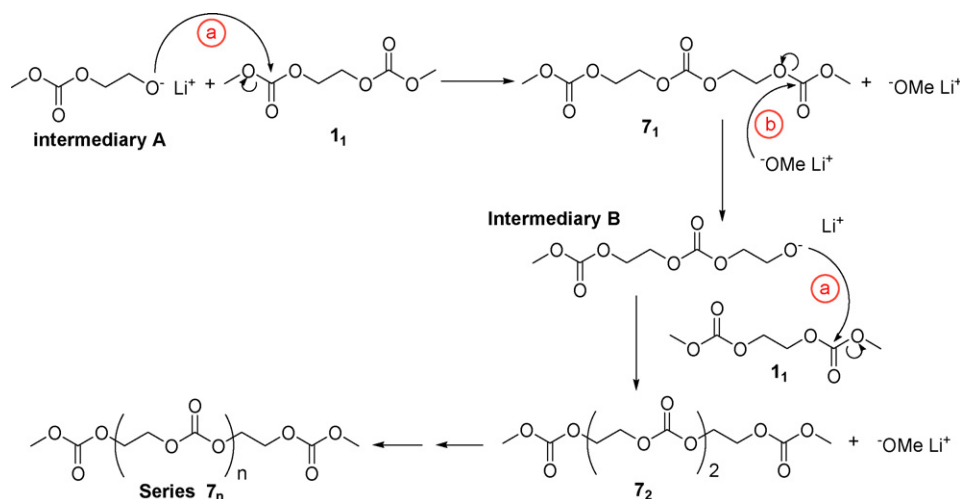
Fig. 7. Reaction scheme for series 7_n formation.
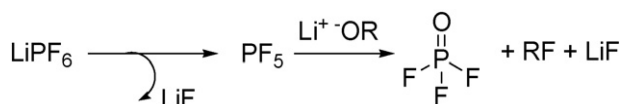
Fig. 8. Reaction scheme for trifluored phosphate formation.

This reaction can proceed n times, to form series 7_n. Interestingly, these reactions consume and regenerate the main reactant MeOLi, which is then catalytic. As far as the phosphate formation is concerned, Radvel et al. [23] stipulated that LiPF$_6$ in the presence of lithium alkoxide forms a first phosphory trifluoride (Fig. 8). POF$_3$ then reacts with more lithium methoxide molecules or with one intermediary molecule (A) to form TMP or POE oligomers with phosphate end groups P (Fig. 9). Note that this last reaction implies the imperative presence of the intermediary A molecule. This molecule, which has been previously envisioned during the 1_1 product formation mechanism, has unfortunately not been characterized yet, owing to its very low steady-state concentration.

3.2. Storage tests for high MeOLi concentrations (1 M)

The ESI-HRMS spectra obtained for the stored samples are represented in Fig. 10. Table 3 gives the accurate masses of the
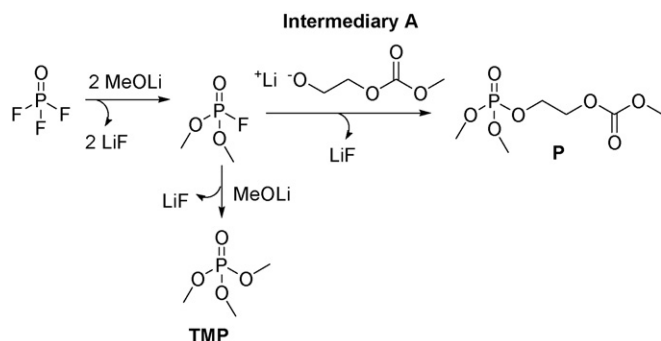
Fig. 9. Reaction scheme for phosphate TMP and P formation.

observed degradation products. The spectrum after 1 day clearly evidences the 1_n series compounds first. Upon increasing the reaction time at 55 °C, the ESI-HRMS peaks corresponding to the longer PEO chains grow at the expense of the shorter ones. Strikingly, it should be noted that the peak corresponding to the 1_1 compound (m/z 185) vanishes, while the peaks corresponding to the 2_n and 3_n series appears which become more prominent after 2-week storage. This drastically contrasts with the low MeOLi concentration storage results as the 1_1 compound was always present, and there has been no evidence of the 2_n and 3_n series. This implies the need for a large MeOLi concentration for the formation of these two series; this is also consistent with their detection in electrolytes recovered from Li/CBO cells cycled at 55 °C for long times (e.g., cumulated capacity of 250 mAh; see Fig. 1) that is to say having large amounts of MeOLi. Again the chronological appearance (e.g., 1_n, then 2_n and 3_n series) is quite coherent with our proposed general mechanism. Following this sequence, it should therefore be noted that only a small amount of series 4_n and 5_n corresponding to POE chains with hydroxyl endings were detected.

Overall, our chemical simulation approach of the MeOLi-electrolyte reactivity has highlighted a strong effect of the MeOLi concentration on the nature of the detected degradation products. A low concentration of MeOLi (10^{-2} mol L^{-1}) stored at 55 °C in the presence of EC/DMC (1/1 w/w)–LiPF$_6$ (1 M) electrolyte mainly leads to the formation of the 1_n series. When increasing the MeOLi concentration (1 M), the formation of the 1_n series was followed by that of 2_n and then 3_n series with a more rapid evolution of the degradation products (as expected for high MeOLi contents). As far as this low concentration solution is concerned, it was also noted that there was no longer an evolution of the degradation after 2 weeks, which seems to indicate that MeOLi was completely consumed, hence confirming the key role of the MeOLi initiator into the electrolyte degradation (Fig. 11).

According to the proposed mechanism, each 1_n, 2_n and 3_n oligomers series would result from an attack of this initiator on the intermediate 1_1 (path 1) and not from a reaction between
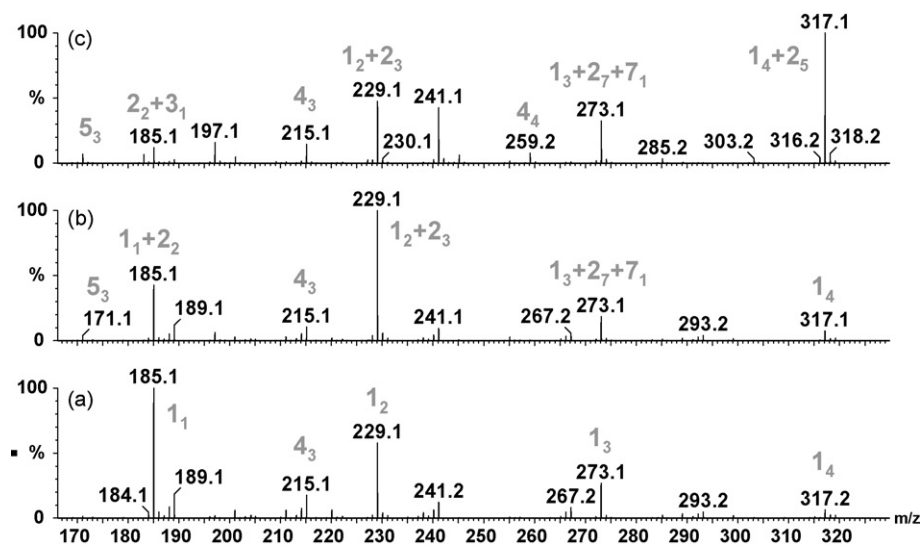
Fig. 10. ESI-HRMS spectra of the EC/DMC (1/1 w/w)–LiPF$_6$ salt (1 M) solution with MeOLi 1 M stored at 55 °C for (a) 1 day, (b) 3 days and (c) 2 weeks.

EC/DMC–LiPF$_6$ and MeOLi (path 2) as proved next.

3.3. Evolution upon storage of the 1_1 compound in the presence of MeOLi (1 M)

To confirm our reaction hypothesis for path 1, another chemical test was carried out; it consists of adding MeOLi (1 M) directly to the commercial 1_1 compound and then leaving the solution to rest at 55 °C for several days. The formation of the
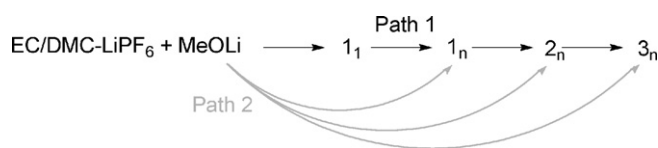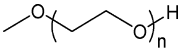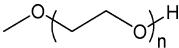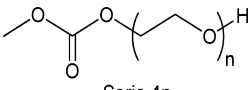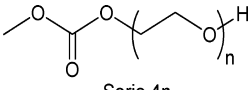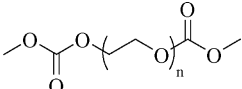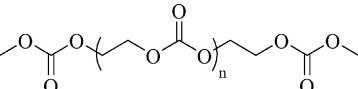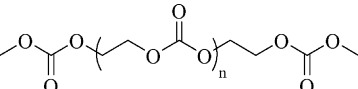
Table 3
Degradation products formed after 2 weeks at 55 °C, in a solution of EC/DMC (1/1 w/w)–LiPF$_6$ salt (1 M) with MeOLi (1 M)

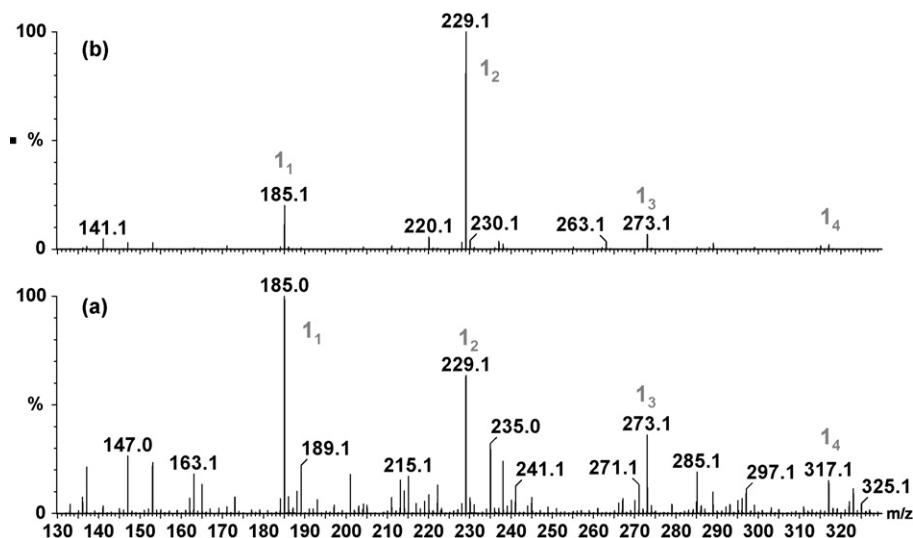| Series	n	m/z	Experimental mass	Calculated mass	Formula
Serie 5n	3	171	171.1195	171.1209	$C_7H_{16}O_4Li$
Serie 5n	2	141	141.1104	141.1103	$C_6H_{14}O_3Li$
	3	185	185.1347	185.1365	$C_8H_{18}O_4Li$
Serie 4n	2	185	185.1001	185.1001	$C_7H_{14}O_5Li$
	3	229	229.1259	229.1263	$C_9H_{18}O_6Li$
	4	273	273.1528	273.1526	$C_{11}H_{22}O_7Li$
	5	317	317.1776	317.1788	$C_{13}H_{26}O_8Li$
Serie 4n	3	215	215.1125	215.1107	$C_8H_{16}O_6Li$
	4	259	259.1369	259.1369	$C_{10}H_{20}O_7Li$
Series 1n	1	185	185.0637	185.0637	$C_6H_{10}O_6Li$
	2	229	229.0897	229.0900	$C_8H_{14}O_7Li$
	3	273	273.1162	273.1162	$C_{10}H_{18}O_8Li$
	4	317	317.1425	317.1424	$C_{12}H_{22}O_9Li$
	5	361	361.1685	361.1686	$C_{14}H_{26}O_{10}Li$
Series 7n	1	273	273.0801	273.0798	$C_9H_{14}O_9Li$
	2	361	361.0960	361.0958	$C_{12}H_{18}O_{12}Li$

Fig. 11. ESI-HRMS spectra of EC/DMC (1/1 w/w)–LiPF$_6$ salt (1 M) solution with (a) 10^{-2} mol L^{-1} of MeOLi after 2-week storage; (b) 1 M of MeOLi after 3-day storage.

1_n, 2_n, 3_n, 4_n, 5_n, and 6_n series was confirmed by mass spectrometry after only 6 days of storage (Fig. 12) implying that the series originated from the 1_1 compound, that is the first degradation product found to be formed in Li/CBO upon discharge down to 0 V.

Besides, the ESI-HRMS spectra of solutions recovered after only 6 days of storage at 55 °C show peaks corresponding to POE chains with hydroxy endings (m/z 157, 201, 245, 289 for the series 6_n and m/z 171, 215, 259 for the series 4_n and 5_n). These peaks were therefore more intense than those detected when MeOLi (1 M) was stored, even for longer times, in the electrolyte at 55 °C. Our belief is that the formation of these hydroxyl PEO-ending groups arises from the hydrolysis of the carbonates functions. This is consistent with water concentration analysis, as deduced by Karl Fisher titration, of 1000 ppm for commercial 1_1 solution as compared to only 40 ppm in our

EC/DMC (1/1 w/w)–LiPF$_6$ (1 M) electrolyte. It should therefore be noted that, after 12 days of storage, the peaks relative to the series 4_n, 5_n, and 6_n almost disappear. Caution has to be exercised in interpreting such disappearance that we believe to be simply the result of two simultaneous reactions involving the nucleophilic attack of the alkyl carbonate function by MeOLi or its hydrolysis. The hydrolysis being limited by the water still present, the peaks corresponding to the series 4_n, 5_n, and 6_n, having at least one OH-ending group are expected to grow until 1000 ppm water present in commercial 1_1 solution has been consumed. Afterwards, with longer storage time, the intensity of these OH-ended capped peaks will not change, while those corresponding to the other series will continue to grow and finally fully mask those of the 4_n, 5_n, and 6_n series.

We highlighted the importance of MeOLi in triggering electrolyte degradation reactions leading to various PEO-based
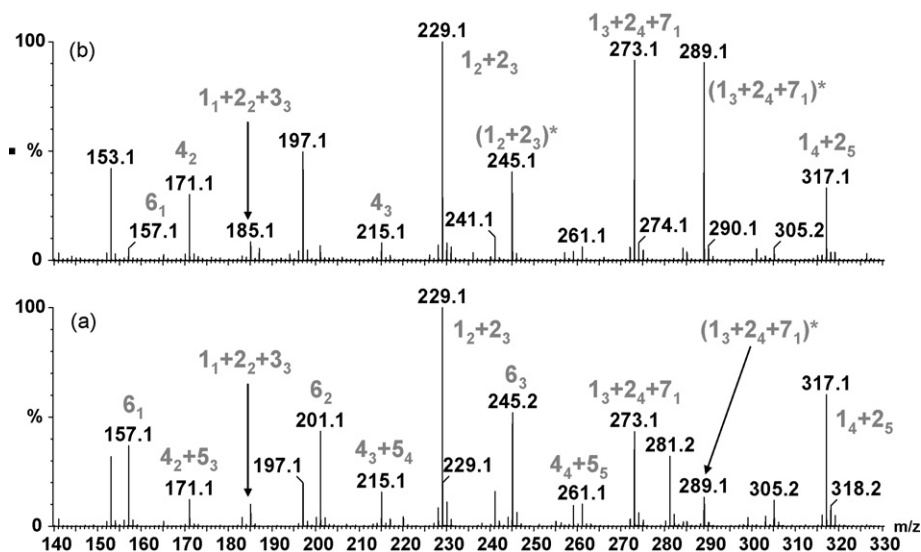

Fig. 12. ESI-HRMS spectra of 1_1 solution with MeOLi (1 M) stored at 55 °C for (a) 6 days; (b) 12 days; ( )* cluster [compound + Na]$^+$.
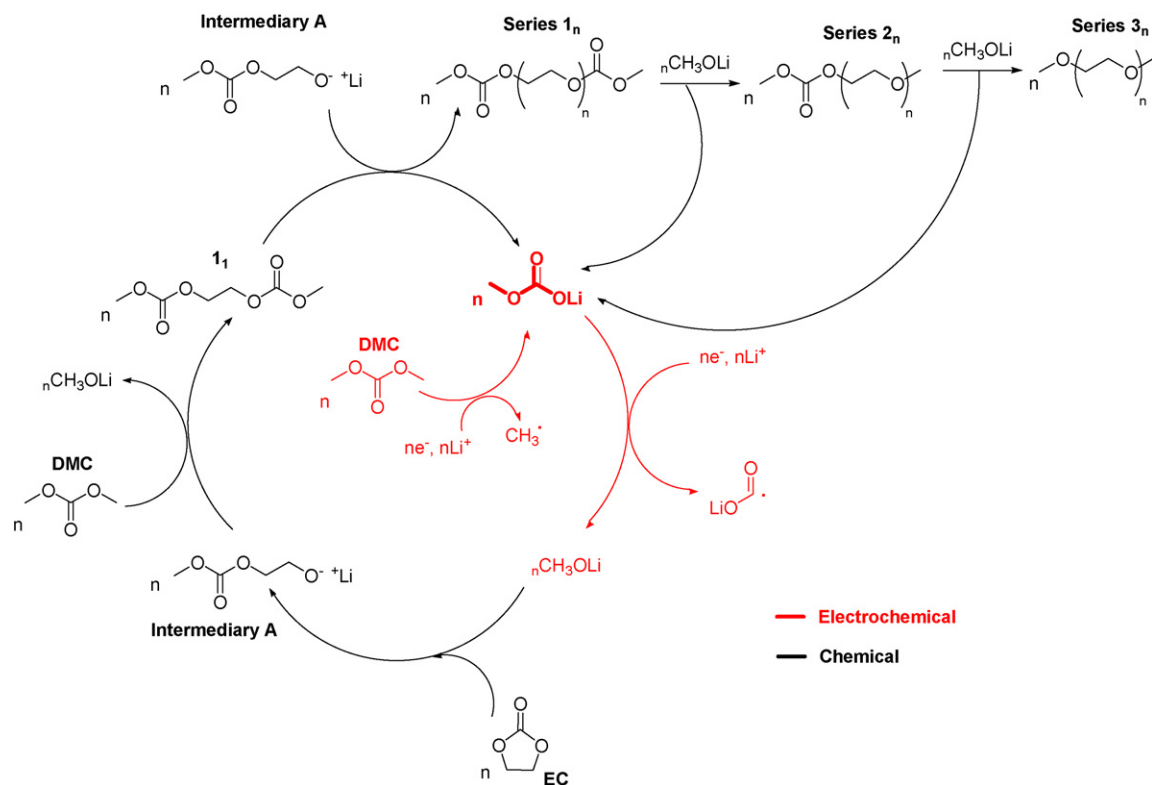
Fig. 13. Reaction scheme for the methyl carbonate formation.

oligomers. However, at this point a legitimate question regards the presence of copious amounts of inorganic species, namely CH_3OCO_2Li, trapped together with the PEO-based oligomers within the glass–fiber separator recovered from long-term cycled Li/CBO cells [18,24]. We should also recall that the formation of lithium alkyl carbonates has so far been reported as resulting from the electrochemical reduction of the corresponding linear carbonated solvent. Accordingly, this implies that its formation should occur at the electrode surface consistent with previous reports stating that such alkyl carbonate was a main component of the SEI layer forming at the surface of the electrode. However, this purely electrochemical pathway fails to account for the presence of CH_3OCO_2Li far apart from the electrode surface, suggesting that its formation might not have a solely electrochemical origin. From the reaction mechanism proposed for the formation of PEO-based oligomers, it seems quite conceivable, according to reaction mechanisms detailed in Fig. 13 and enlisting the lengthening of the series 1_n together with the formation of the series 2_n and 3_n, that lithium alkyl-carbonate can also form chemically.

3.4. Chemical formation of CH_3OCO_2Li

The best way of probing this chemical path was to further exploit our previously presented chemical approach; besides leading to the formation of the PEO series it has revealed at the surface of the MeOLi saturated electrolyte solution, a white fluffy gel that can be precipitated in the presence of acetonitrile. After several washings with this solvent, a white powder was recovered and analyzed by IR and NMR. By comparing

the collected IR spectrum with the IR signatures of pure salts that we had synthesized in house, we could deduce the presence of CH_3OCO_2Li (Fig. 14) in the recovered white powder. Such assignment was further confirmed by both ^1H NMR and ^{13}C NMR analyses with namely the appearance of a signal at 3.21 ppm for the ^1H NMR and of two signals at 49.18 and 161.89 ppm for the ^{13}C characteristics of CH_3OCO_2Li [19]. Furthermore, based on ^1H NMR signal intensity, we deduced that CH_3OCO_2Li was the main constituent of the powdery product. We did not attempt to identify the other minor prod-
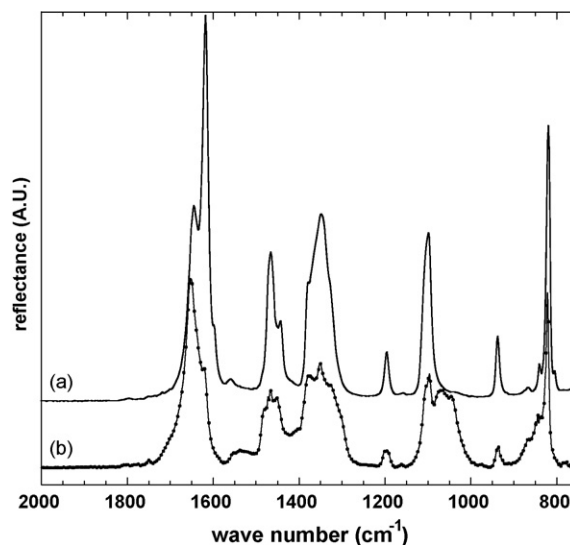

Fig. 14. Infrared spectrum of (a) pure CH_3OCO_2Li and (b) the white powder.

uct(s) as its NMR signature was too weak. Altogether this experiment provides convincing evidences for the concomitant chemical formation of CH_3OCO_2Li and PEO-based oligomers when an EC/DMC (1/1 w/w)–$LiPF_6$ salt (1M) electrolyte mixture is stored in the presence of MeOLi at 55 °C. As the MeOLi can be electrochemically generated, the surprising large amount of CH_3OCO_2Li detected in the separator and recovered from long-term cycled Li/CBO cells, is no longer a surprise. Indeed, according to our proposed mechanism, CH_3OCO_2Li generated from an electrochemical reduction of DMC, is continuously consumed via a second electrochemical reduction step; this leads to the formation of MeOLi that, once in contact with the electrolyte, will chemically react via a nucleophilic attack of the carbonate function leading to the 1_n, 2_n 3_n series and an accumulation of the alky-carbonate salt (Fig. 13). As this salt is weakly soluble in carbonated electrolytes, it will accumulate within the cell separator causing it to dry-up with the end result being a deterioration of the extended cell-cycling performance, consistent with our observations.

3.5. Generalization to other cyclic/linear carbonate-based electrolyte

Having established a solid and meaningful mechanism related to the degradation of the EC/DMC–$LiPF_6$ electrolyte, we checked whether it could be applied to other carbonates electrolyte mixtures. We first changed the nature of the cyclic carbonate (e.g., using PC instead of EC). Similar high resolution mass spectrometry investigations were performed on (1) solutions resulting from 55 °C storage of MeOLi in the presence of PC-based electrolyte and (2) separators recovered from Li/CBO cells cycled for a long time and using PC/DMC (1/1 w/w)–$LiPF_6$ salt (1 M) electrolytes. In both cases we could deduce, in agreement with our earlier study [2], the presence of polypropylene glycol (PPG) chains having ending groups similar to those previously detected with the EC-based electrolyte. This implies that our proposed global electrolyte decomposition mechanism holds regardless of whether we use either EC or PC as cyclic carbonate.

Next, as DMC was shown, through its electrochemical reduction, to initiate the polymerization process, it was interesting to evaluate the difference brought by the substitution of DMC for DEC when cycled in somewhat similar conditions.
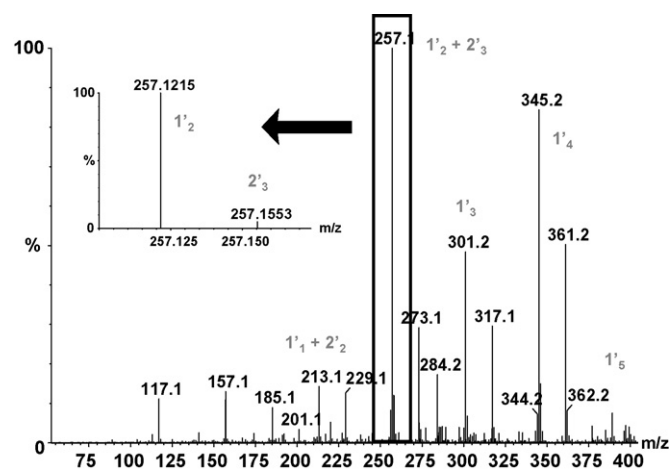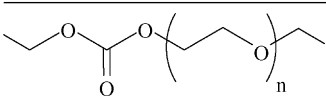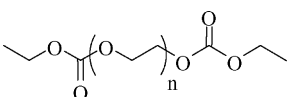

Fig. 15. Mass spectrum obtained with EC/DEC (1/1 w/w)–$LiPF_6$ salt (1 M) electrolyte after a "long-term cycling" (total accumulated discharge capacity of 140 mAh) at 55 °C.

To carry out this study, Li/CBO half-cells using an EC/DEC (1/1 w/w)–$LiPF_6$ salt (1 M) electrolyte were cycled at 55 °C for more than 200 cycles, and stopped when their cumulated discharge capacity reached 140 mAh. Afterwards, the cells were disassembled in a dry box, and the recovered separator was washed with acetonitrile. The supernatant was analyzed by high resolution mass spectrometry (Fig. 15). The collected spectra show numerous signals, implying the existence of numerous degradation products whose accurate masses and corresponding structural formula are reported in Table 4. This analysis confirms the formation of the $1'_n$ and $2'_n$ series, which differ from the 1_n and 2_n series previously encountered with DMC-based electrolyte by having now an ethyl rather than a methyl termination group; the latter $2'_n$ series being the less predominant as the intensity of its peaks is much weaker than that of isobaric peaks corresponding to the $1'_n$ series (inset Fig. 15). Interestingly, the first member of our $1'_n$ series ($1'_1$) is the diethyl 2,5-dioxahexane dicarboxylate molecule (termed as DEDOHC), whose formation was suggested by Ogumi and co-workers [17] via a mechanism similar to that used by this team for the growth of the 1_1 molecule (e.g., DMDOHC). From further analysis of the ESI-HRMS spectra, we should note that the number of POE oligomers is greater for the $1'_n$ series ($n = 1$–5) than for the $2'_n$ series ($n = 2, 3$) suggesting its earlier formation.

Table 4
Degradation products present after a "long-term cycling" (140 mAh) in the cell using EC/DEC (1/1 w/w)–$LiPF_6$ salt (1 M) electrolyte at 55 °C

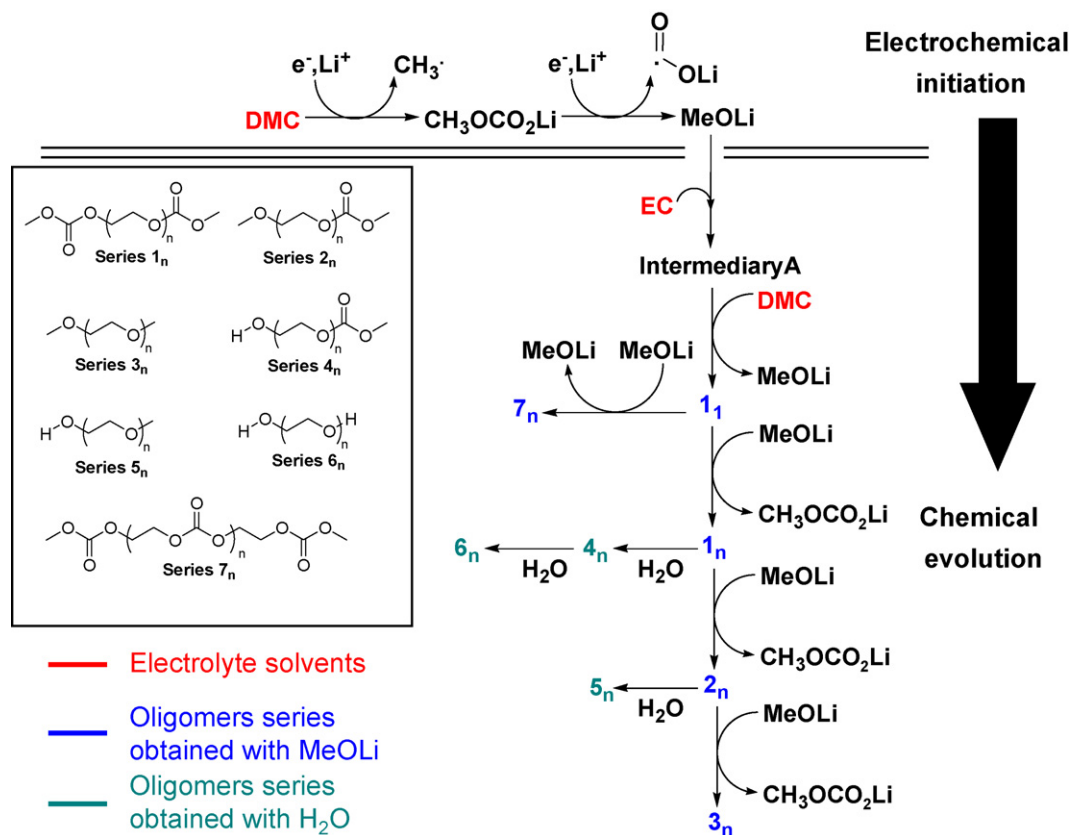| Series	n	m/z	Experimental mass	Calculated mass	Formula
Series $2'_n$	2	213	213.1314	213.1314	$C_9H_{18}O_5Li$
	3	257	257.1553	257.1576	$C_{11}H_{22}O_6Li$
Series $1'_n$	1	213	213.0947	213.0950	$C_8H_{14}O_6Li$
	2	257	257.1215	257.1213	$C_{10}H_{18}O_7Li$
	3	301	301.1477	301.1475	$C_{12}H_{22}O_8Li$
	4	345	345.1733	345.1737	$C_{14}H_{26}O_9Li$
	5	389	389.1990	389.1999	$C_{16}H_{30}O_{10}Li$

Fig. 16. Global scheme of electrochemical/chemical low-potential degradation processes described for EC/DMC (1/1 w/w)–LiPF$_6$ salt (1 M) electrolyte.

Besides, it is worth mentioning that the degradation reaction is not as advanced as expected for such 140 mAh-cycled cell, but rather comparable with the degradation stage of a 55 °C-cycled cell, using EC/DMC (1/1 w/w)–LiPF$_6$ (1 M) electrolyte, and having a discharge cumulated capacity of solely 55 mAh. It can then be concluded that the substitution of DMC for DEC appreciably slows down the degradation process upon cycling. The explanation may lie in the formation and the reactivity of EtOLi, which could be different from that of MeOLi. Chemical simulations tests are being performed to confirm our hypothesis.

4. Conclusions

We have revisited the low-potential degradation mechanisms of carbonate-based electrolytes in Li-based batteries. On the basis of chemical simulation tests followed by thorough ESI-HRMS, IR, and NMR analytical studies, we have put forward a novel global reaction mechanism path (Fig. 16). This mechanism successively accounts for the electrochemical reduction of DMC and the multi-step chemical reaction of the resulting MeOLi with the electrolyte. The latter enables to account for both the chronological appearance of the different 1_n, 2_n and 3_n POE oligomers series and the presence of CH_3OCO_2Li salt in separators recovered from Li/CBO cells cycled at 55 °C for a long time. This is the first time that the chemical formation of such a salt, known to form electrochemically under reduction in

Li-cells, was predicted and unambiguously confirmed by complementary IR and NMR measurements. We must also stress that our newly established electrolyte degradation mechanism is not specific to an EC-DMC-based electrolyte as it was successfully applied to account for the degradation products formed during the long-term cycling of Li/CBO electrode; this was done by using either EC/DEC (1/1 w/w)–LiPF$_6$ salt (1 M) or PC/DMC (1/1 w/w)–LiPF$_6$ salt (1 M) instead of EC/DMC electrolytes. Similarly, on the basis of this proposed mechanism, one can easily explain why the presence of the cyclic (EC, or PC) or the acyclic (DMC or DEC) alone does not lead to the formation of polymers. The reason being that in presence of a cyclic carbonate one cannot have the formation of the alkyl carbonate salt then RO$^-$, Li$^+$ necessary to trigger the degradation mechanism; whereas with an acyclic one we can never trigger the formation of the intermediary A species (Fig. 16) the reason why we solely witnessed the formation of TMP and MeOLi [2]. Importantly, it should be added that the proposed mechanism still holds regardless of the nature of the electrolyte salt, except for the products arising from LiPF$_6$ breakdown, the type of conversion or alloying reactions electrodes that we have been experimenting, as it will be reported in a forthcoming paper. Overall, this new understanding of electrochemically/chemically-driven electrolyte degradation mechanisms is expected to have a strong impact on future studies trying to design more robust carbonate-based electrolyte formulations, a necessary requirement for the development of safer Li-ion batteries.

References

[1] E. Peled, J. Electrochem. Soc. 126 (1979) 2047–2051.
[2] S. Laruelle, S. Pilard, P. Guenot, S. Grugeon, J.-M. Tarascon, J. Electrochem. Soc. 151 (8) (2004) A1202–A1209.
[3] R. Dedryvère, S. Laruelle, S. Grugeon, P. Poizot, D. Gonbeau, J.-M. Tarascon, Chem. Mater. 16 (2004) 1056–1061.
[4] S. Grugeon, S. Laruelle, L. Dupont, F. Chevallier, P.L. Taberna, P. Simon, L. Gireaud, S. Lascaud, E. Vidal, B. Yrieix, J.-M. Tarascon, Chem. Mater. 17 (2005) 5041–5047.
[5] J. Vollmer, L. Curtiss, D. Visser, K. Amine, J. Electrochem. Soc. 151 (1) (2004) A178–A183.
[6] D. Aurbach, M. Laroux, P. Faguy, E. Yeager, J. Electrochem. Soc. 134 (1987) 1611–1620.
[7] D. Aurbach, Y. Gofer, M. Ben-Zion, P. Aped, J. Electroanal. Chem. 339 (1992) 451–471.
[8] D. Aurbach, Y. Ein-Ely, A. Zaban, J. Electrochem. Soc. 141 (1994) L1–L3.
[9] D. Aurbach, Y. Ein-Ely, O. Chusid, Y. Carmeli, M. Babai, H. Yamin, J. Electrochem. Soc. 141 (1994) 603–611.
[10] D. Aurbach, Y. Ein-Eli, B. Markovsky, A. Zaban, S. Luski, Y. Carmeli, H. Yamin, J. Electrochem. Soc. 142 (1995) 2882–2890.
[11] G. Zuang, K. Xu, H. Yang, R. Jow, P. Ross, J. Phys. Chem. B 109 (2005) 17567–17573.
[12] K. Xu, G. Zuang, J. Allen, U. Lee, S. Zhang, P. Ross, R. Jow, J. Phys. Chem. B 110 (2006) 7708–7719.
[13] E. Takeuchi, H. Gan, M. Palazzo, R. Leising, S. Davis, J. Electrochem. Soc. 144 (1997) 1944–1948.
[14] D. Aurbach, A. Zaban, Y. Ein-Eli, O. Weissman, B. Chusid, B. Markovsky, M. Levi, E. Levi, A. Schechter, E. Granot, J. Power Sources 68 (1997) 91–98.
[15] H. Yoshida, T. Fukunaga, T. Hazama, M. Terasaki, M. Mizutani, M. Yamachi, J. Power Sources 68 (1997) 311–315.
[16] Y. Ein-Ely, Electrochem. Solid-State Lett. 2 (5) (1999) 212–214.
[17] T. Sasaki, T. Abe, Y. Iriyama, M. Inaba, Z. Ogumi, J. Power Sources 150 (2005) 208–215.
[18] L. Gireaud, S. Grugeon, S. Laruelle, S. Pilard, J.-M. Tarascon, J. Electrochem. Soc. 152 (5) (2005) A850–A857.
[19] R. Dedryvère, S. Laruelle, S. Grugeon, L. Gireaud, J.-M. Tarascon, D. Gonbeau, J. Electrochem. Soc. 152 (4) (2005) A689–A696.
[20] A.M. Andersson, K. Edström, J. Electrochem. Soc. 148 (10) (2001) A1100–A1109.
[21] S. Sloop, J. Kerr, K. Kinoshita, J. Power Sources 119–121 (2003) 330–337.
[22] S. Grugeon, S. Pilard, P. Guenot, J.-M. Tarascon, S. Laruelle, Anal. Chem. 78 (11) (2006) 3688–3698.
[23] B. Radvel, K.-M. Abraham, R. Gitzendanner, J. DiCarlo, B. Lucht, C. Campion, J. Power Sources 119–121 (2003) 805–810.
[24] R. Dedryvère, L. Gireaud, S. Grugeon, S. Laruelle, J.-M. Tarascon, D. Gonbeau, J. Phys. Chem. B 109 (2005) 15868–15875.